IEEE Access
Multidisciplinary | Rapid Review | Open Access Journal

Received 13 December 2022, accepted 25 December 2022, date of publication 27 December 2022,
date of current version 12 January 2023.

Digital Object Identifier 10.1109/ACCESS.2022.3232697

RESEARCH ARTICLE

Reconfigurable Plasma Composite Absorber Coupled With Pixelated Frequency Selective Surface Generated by FD-CGAN

MENGJIE YU[1,2], HAITAO WANG[1], XIANGXIANG GAO[1,2], XI REN[1], ZUNYI TIAN[1], HENGGAO DING[3], AND ZHONGYU HOU[1]

[1]National Key Laboratory of Science and Technology on Micro/Nano Fabrication, Shanghai Jiao Tong University, Shanghai 200240, China
[2]Department of Micro/Nano Electronics, School of Electronic Information and Electrical Engineering, Shanghai Jiao Tong University, Shanghai 200240, China
[3]Chinese Academy of Engineering, Beijing 100088, China

Corresponding author: Zhongyu Hou (zhyhou@sjtu.edu.cn)

This work was supported in part by the National Natural Science Foundation of China under Grant 60906053, Grant 61204069, Grant 61274118, Grant 61306144, Grant 61504079, and Grant 11605112; and in part by the Scientific and Innovative Action Plan of Shanghai under Grant 15DZ1160800 and Grant 17XD1702400.

ABSTRACT Conventional plasma absorbers are challenging to obtain high electron density and sizeable spatial scale for effective absorption while meeting the applied requirements of low profile and low power consumption. Although the frequency selective surface (FSS) has proved to realize a lower profile of plasma absorber with some empirical patterns adequately, the issue of the FSS design matching the dispersion distribution of complicated plasmas is still in suspense. A reverse prediction method referenced as the forecast and design Conditional Generative Adversarial Network (FD-CGAN) is proposed to generate a pixelated FSS between double-layer plasma periodic arrays. The reflection attenuation characteristics examined by experiments show that the addition of the FSS makes the coupling absorption effect surpass that of either pixelated FSS or plasma solely. Measurements in reconfigurable working modes and array arrangements demonstrate that the proposed configuration maximizes absorption effectiveness in the same profile, accompanied by the simulation. An interfacial void model is proposed to assist the design of the composite absorbing structure, together with an equivalent circuit for the hybrid absorber including periodic patterns with stochastic distribution characteristics, which analyze the absorption effect of the composite structure. The study provides a new approach for various microwave applications, including multilayer radar-absorbing structures, plasma-based stealth technology, and reconfigurable filters.

INDEX TERMS Microwave absorption, plasma periodic structures, pixelated frequency selective surface, generative adversarial network, reconfigurable absorber.

I. INTRODUCTION

As a dispersive and lossy medium, the collisional plasma has a complex dielectric constant and can be used as an effective absorber of electromagnetic (EM) waves in a wide range of frequencies [1]. Besides exhibiting high attenuation over a large bandwidth, another advantage of a plasma absorber has also been emphasized: thanks to the sub-nanosecond collisional energy transition processes among particles in plasmas [2], the spatial refractivity of plasmas is tunable and fast-switchable, so its reconfigurability can be achieved by the electrical control [3]. Three particularities of plasma place technical demands on the preparation of microwave-active plasmas that are difficult to implement: the absorption capacity of a collisional plasma is determined by the oscillation and collision behavior of electronic dipoles [4], i.e., the high absorption capacity depends on the plasma with high densities in the certain wavelength range; the scale of volumetric plasma needs to be large enough compared to the wavelength of the incident EM wave [5]; and achieving high electron

The associate editor coordinating the review of this manuscript and approving it for publication was Jiachen Yang.

number density is unavoidably accompanied by the high power and heating scenarios [6].

It has been discovered that the inclusion of the frequency selective surface (FSS) can circumvent the above limitations to achieve high absorption with low power consumption and low profile. A large-area, lightweight, conformal plasma device which was electrically excited by FSSs was proposed to interact with X-band microwave energy [7]. An equivalent circuit model was demonstrated to analyze the wideband absorber with the combination of plasma and resistive FSS [8]. Payne et al. have carried out a series of studies on the low-profile plasma-based tunable absorber integrated with FSS [9], [10], [11]. In addition to forming the controlled wavefront distribution on a large scale, FSS can be coupled with plasmas to modulate the phase cancellation of EM waves. It seems to convert part of the bulk plasma into a thin, low-power, and highly controllable metallic periodic structure, which can be considered as a ''quasi-plasma'' with high density, yielding greater absorption effects while reducing the thickness of the plasma itself.

The conventional design process of FSS is empirical and usually consists of model design, parameter sweeping, and optimization, in which assembled patterns are mainly restricted to linear type, loop type, solid patch, or mixture, allowing for little flexibility in the optimizing procedure [12], [13]. In addition, under the condition that the interlayer coupling of the composite absorbing structure cannot be neglected, synthesizing the satisfactory FSS with adaptive features of coupling with plasma becomes difficult [14]. Generative adversarial networks (GANs) of Deep learning (DL) method [15], which are characterized by training a pair of networks in competition with each other, have been proposed to innovate the design of an FSS to match the desired scattering properties [16], [17], [18]. Compared with other DL-based design approaches, GANs can partly solve the information loss of the convolution neural networks and generate new samples that are similar to those in the dataset but have a singularity, which indicates the advantage in generating unpredictable periodic structures [19]. Hence, the approach can be effective in matching the dispersion distribution of complicated plasmas during the design of a composite structure, which has no attempt to be found in the literature. Moreover, to increase the degrees of freedom of the structure, a pixelated pattern is used to exhibit great flexibility in the optimization procedure due to the use of binary inversion of pixel values under the certain frequency response requirement by splitting the unit cell up into a grid of sub pixels [20], [21].

The paper presents a reconfigurable microwave absorber composed of plasma arrays and the pixelated frequency selective surface for the first time. We propose an adaptive reverse design strategy with the conditional GAN model to optimize pixelated structures, which is enabled to generate optimal geometric patterns to reduce the return wave of the hybrid structure. It is found that the coupled structure has induced a wideband attenuation effect and reconfigurable-switching effect. The reflection characteristics of the absorber and pixelated FSS or plasma solely are explored using a free space measurement facility, accompanied by working modes and array arrangements. The reason for the intensive coupling effect is discussed through simulation analysis and the lumped circuit model. The method exhibits the potential to control the propagation of microwaves via a reconfigurable hybrid plasma system.

II. EXPERIMENTAL SETUP AND METHOD

A. CONFIGURATIONS OF THE PROPOSED RECONFIGURABLE COMPOSITE ABSORBING STRUCTURE

Figure 1(a) provides the experimental diagram of the absorbing structure and the measuring system. The experiment is conducted in the anechoic chamber. The propagation of free space EM waves is realized by a pair of broadband horn antennas (LB-10180-NF, A-INFO Co., Ltd.) as the microwave source and receiver, which has frequency ranges of 1-18 GHz and the gain of 11 dB. The antennas are connected to an Agilent 8720ES vector network analyzer to measure the reflection characteristics. The distance from the symmetrical antennas to the absorber is about 110 cm, and the structure is fixed above the foam holder with the dielectric constant considered as 1. It is noticed that the electric field is polarized along the y-axis, which is transverse to the axis along plasma cylinders. The EM wave propagates in the negative direction of the z-axis, that is, normal incident on the target. The time-gating method is used to eliminate the influence of unnecessary scattering in free space.

The top view of the proposed composite absorbing structure under the working state is illustrated in Fig. 1(b). In order to further reduce scattering noise, the absorbing wedges hide the electrical connection at the tube tip and leave a 20×20 cm testing window. As shown in Fig. 1(c), the absorber is composed of a multi-layer composite structure, with the sequence from top to bottom of ''top plasma layer - pixelated FSS layer - bottom plasma layer - metallic ground''. The thickness of the metallic ground is much larger than the skin depth, reflecting all the incident electromagnetic waves, which can be considered as perfect electrical conductor (PEC). Each layer of plasma arrays consists of twelve individual discharge tubes with quartz enveloped ($\varepsilon = 3.8$), which are 15 mm and 13 mm in outer and inner diameter, respectively. The visible plasma length of discharge tubes filled with low-pressure argon and mercury vapor is 200 mm, and the distance between each tube is 2 mm. Each cylindrical plasma tube is driven individually by an AC ballast, which controls the plasma state by adjusting the plasma density and frequency. In accordance with the triangular-shaped current waveform of the discharge tube, the root mean square (RMS) current I_{RMS} is 154.73 mA at a frequency of 22.68 kHz.

It is well known that there are two characteristic parameters of plasmas, including the plasma density and the momentum transfer collision frequency of the plasma electrons. A gas discharge model is used to estimate the resulting plasma density in the system [22]. The relationship between the measured I_{RMS} and the average electron

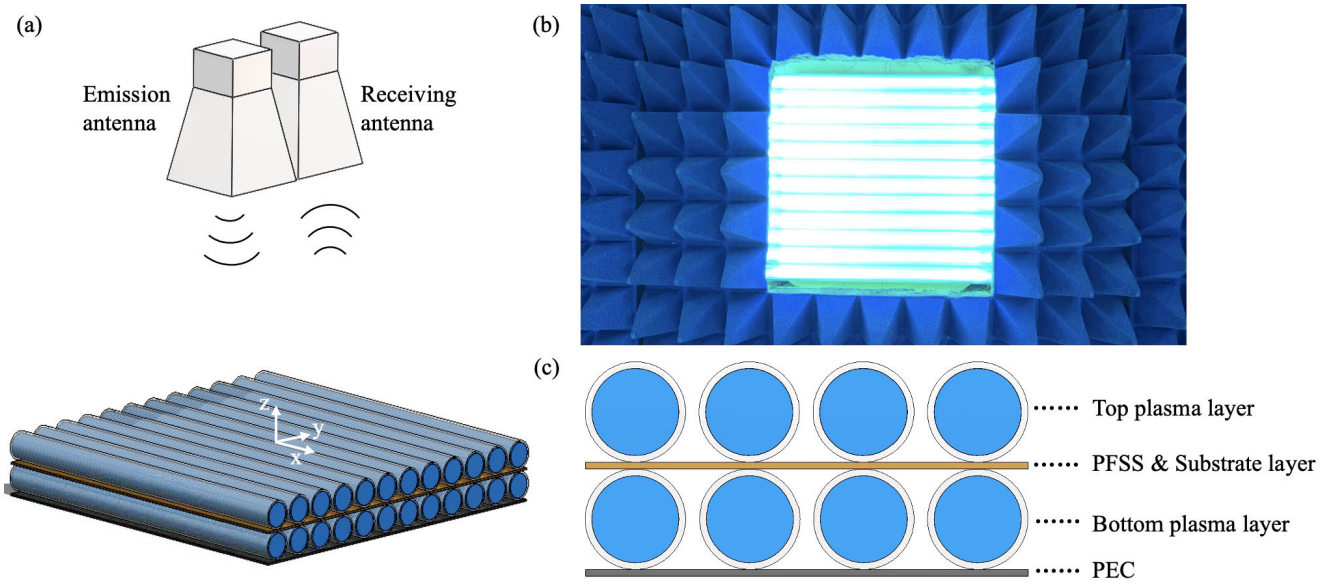

FIGURE 1. The designed experimental system: (a) schematic of experimental apparatus and measuring system, (b) photograph of the test zone with absorbing wedges surrounding, and (c) side view of part of the proposed structure.

density n_e is given as follows

$$n_e = \frac{I_{RMS}}{eA\mu_d}, \tag{1}$$

where e is the charge of an electron, A is the inside cross-sectional area of each discharge tube, and μ_d is the electron mobility. μ_d is calculated through the Boltzmann equation using BOLSIG+ [23], and the required time-averaged reduced electric field (E/N) is obtained from the discharge voltage and the total pressure of the mixed gas. Hence, the estimated electron density is roughly between 7.54×10^{16} m^{-3} and 1.23×10^{17} m^{-3}, which is in the range of the conventional mercury-based fluorescent lamp plasma [24].

As a lossy dispersive dielectric material, plasma has the dielectric constant described by the Drude model

$$\varepsilon_p = 1 - \frac{\omega_p^2}{\omega(\omega - j\nu)} = 1 - \frac{\omega_p^2}{\omega^2 + \nu^2} - j\frac{\nu}{\omega}\frac{\omega_p^2}{\omega^2 + \nu^2}, \tag{2}$$

where ω_p is the plasma frequency, ω is the EM wave frequency, and ν is the momentum transfer collision frequency of the plasma electrons, which is about the value of $\nu = 5.6 \times P(torr) \times 10^9(Hz)$ based on the low-pressure argon glow discharge technology [25]. In the above equation, ω_p is a function of the electron density

$$\omega_p = \sqrt{\frac{n_e e^2}{m_e \varepsilon_0}}, \tag{3}$$

with m_e being the electron mass and ε_0 being the vacuum permittivity. Using the above relation, the propagation constant $k(\omega)$ for EM waves in a collisional plasma can be expressed as [26]

$$k(\omega) = \frac{\omega}{c}\sqrt{\varepsilon_p}, \tag{4}$$

where c is the speed of light for vacuum.

B. FD-CGAN MODEL AND GEOMETRICAL CONSTRUCTION

Replacing the traditional design procedure of periodic patterns on FSSs, the FD-CGAN architecture, which combines the deep convolutional neural network (CNN) and the generative adversarial network (GAN), enables forward prediction of the S-parameters and designs geometrical patterns inversely under different frequency response requirements. The training and testing datasets of the model are constructed with the full wave simulator. Each square patch is represented by a binary bit, where "1" indicates the presence of PEC metal, and "0" indicates the absence. The coded patterns build a unique map from spatial terms to numerical values, simplifying the traditional modeling process. Figure 2 provides an overview of FD-CGAN architecture, which is a semi-supervised learning model based on game theory. It comprises three different networks: the generator (G), the discriminator (D), and the predictor (P). The generative neural network G generates synthetic data represented as pixelwise images from the random noise and real spectra, and the discriminative neural network D estimates the probability that the sample came from the training data rather than G. If the D identifies a fake structure, the results are backpropagated to G, which the learnable parameters and growth rules will be adjusted to reduce the error. While if the D cannot distinguish errors of the data distribution between the fake and real structures, the information of matrices will be fed to the predictive neural network P. The P is a pre-trained network for a given pattern as its input, and a fake reflection spectrum is generated as the output, which is learning to be close to the real response continuously [27]. Furthermore, extensive experiments demonstrate that the pixelated images generated by the proposed FD-CGAN model can obtain the preset electromagnetic responses.

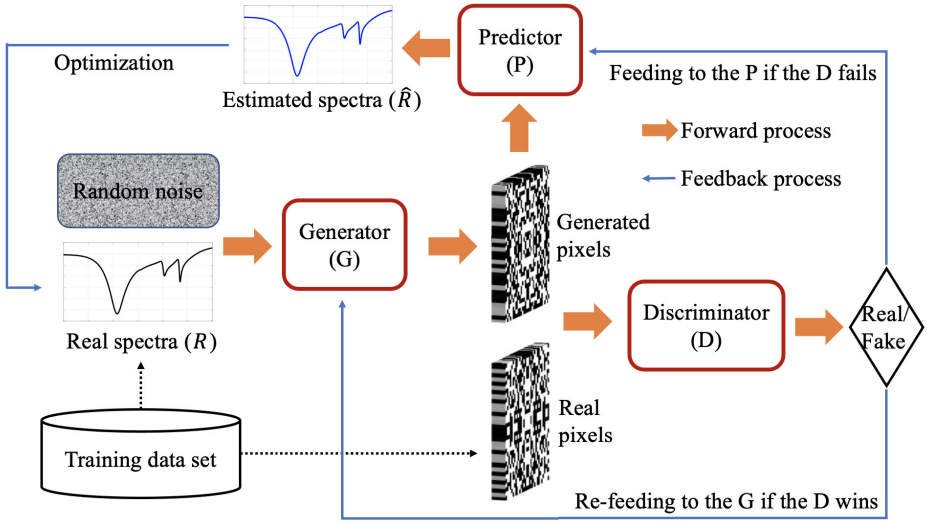

FIGURE 2. The complete architecture of the proposed FD-CGAN model includes a generator (G), a discriminator (D), and a predictor (P). In the process of training G, the generated patterns vary depending on the feedback from D and P. The distribution of pixel points that meets the reflection response expectations is captured with iterations.

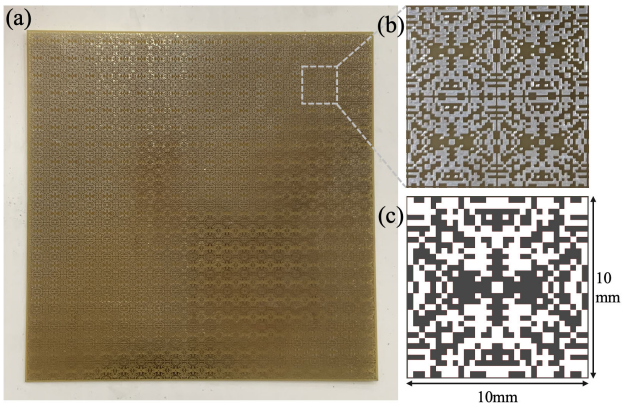

FIGURE 3. (a) FSS screen structure with the unit cells of 20 × 20; (b) Detailed view of four units in FSS screen; (c) Unit cell geometry with the size of 10 mm by 10 mm, in which white areas indicate the metal.

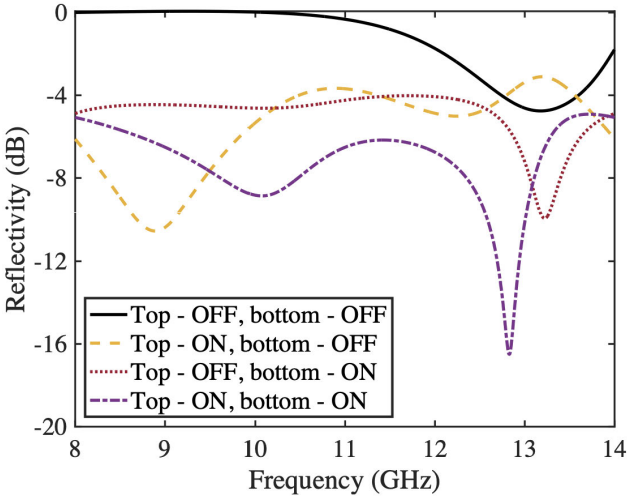

FIGURE 4. Reflection spectrum comparisons for various states of plasma arrays with double layers in experimental measurement. The "OFF" state means the plasma layer is not working, while the "ON" state is the opposite.

The optimized pixelated FSS structure, including unit cell and screen geometry, is shown in Fig. 3. The fabricated FSS contains 20 × 20 elements on the substrate, and the unit cell area is split up into a 32 × 32 grids of pixels. The standard PCB process is done on the upper surface of a 1 mm FR-4 substrate with a permittivity of 4.4 and a loss tangent of 0.02. The other design parameters include the wire trace width $\omega =$ 0.315 mm, the thickness of the copper clad $t_\omega = 30$ μm, and the periodic separation $s = 10.2$ mm.

III. RESULTS AND DISCUSSION

A. REFLECTION CHARACTERISTICS OF PLASMA ARRAYS OR PIXELATED FSS SOLELY AND THE COUPLED STRUCTURE

The reflection spectrum of double-layer plasma arrays solely is demonstrated in Fig. 4. Notice that the top plasma layer is closer to the microwave source than the bottom one. Quartz tubes that exist throughout the experiment serve as the structural framework, which induces a slight resonance of −4.8 dB located around 13.2 GHz. It can be attributed to the phase modification and scattering caused by the dielectric constant and shape of quartz tubes, respectively. The other three states have broadband attenuation across the test band. Comparing the single layer of the "ON" state, the resonance peak of −10.5 dB located around 8.9 GHz appears when the top plasma layer is excited. In contrast, the largest peak occurs at 13.2 GHz with the value of -10 dB as the bottom layer is excited. In the case of both discharge layers turned on, the intense resonance effect appears at 12.8 GHz with the value of −16.5 dB. The absorption peaks are the result of multiple reflections between double-layer plasma arrays, which are due to the cavity resonance effect and collisional absorption [28]. One can see that due to the cavity resonance

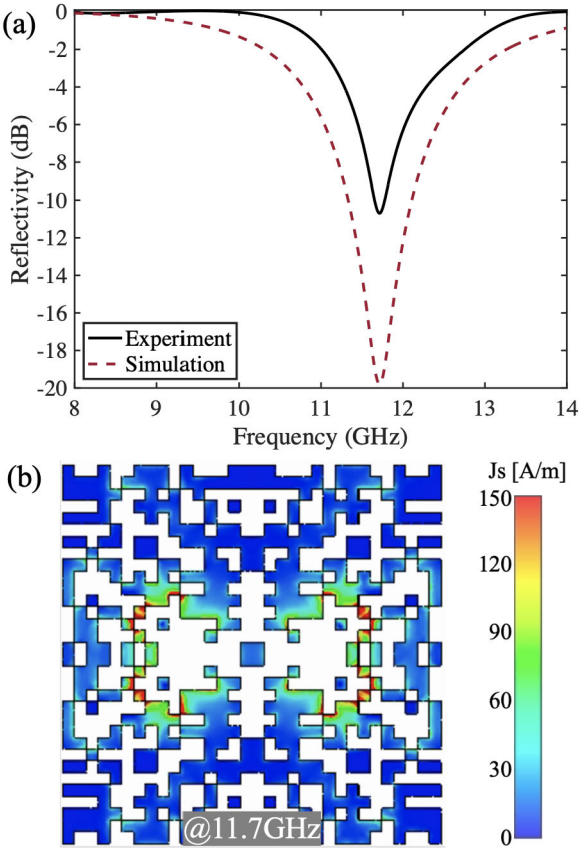

FIGURE 5. (a) Experimental measured and simulated reflection spectrum of the designed pixelated FSS alone; (b) The surface current distribution on the unit cell at the resonance.

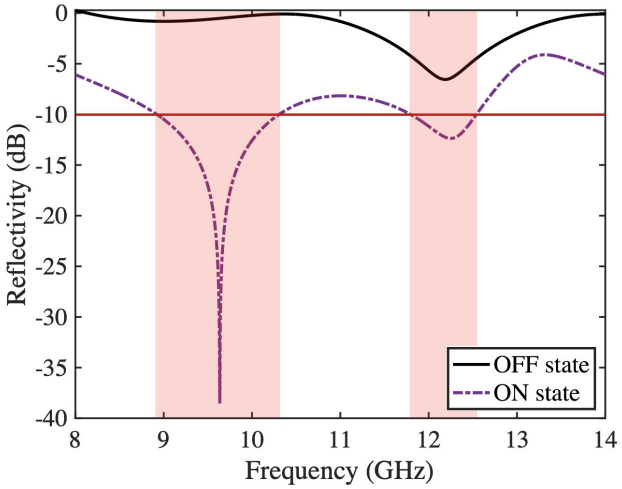

FIGURE 6. Reflection response of the proposed composite structure for two states in experimental measurement. The "OFF" state means plasma layers are not working, while the "ON" state is the opposite. The parts marked in red are absorption bands below −10 dB.

effect of enclosed plasmas, the attenuation and layers are no longer a simple linear relationship. It can be inferred that there is a large density gradient at the boundary of plasma arrays, and the interface of plasmas and air is not completely satisfied with the impedance matching condition, leading to an attenuation of the incident wave.

The reflectivity is calculated over a frequency range from 8 to 14 GHz, and use minimum/maximum tolerable values to define the solution's fitness. Figure 5(a) presents the theoretically calculated and experimentally measured reflection spectrum of the pixelated FSS with constraints. Despite the existence of value differences, the experimental result shows a congruent changing trend with the simulated one, both exhibiting the resonance at around 11.7 GHz. The experimental curve displays the attenuation peak of -10.7 dB, which is a reduction of +46.0 % from the simulated one in the absolute value. Deviations in resonant frequencies and attenuation are due to the difference between the finite measurement and the infinite simulation.

Figure 5(b) depicts the surface current distribution on the pixelated unit cell at the resonant frequency of 11.7 GHz. It is observed that the magnetic field distribution of the cell where the resonances around f = 11.7 GHz originates from the surface current flow inside the cell rather than on the boundaries bordering other cells. In other frequency ranges, the induced surface current becomes remarkably weak. One can see that the intensity of the surface current distribution and the fringing field that give rise to the capacitive effect are low at the resonant frequency of 11.7 GHz, which is an advantage from a power-handling point of view [29].

With the consideration of the adaptive features of coupling with plasma, a composite absorbing structure composed of plasma arrays and the pixelated FSS is designed. The reflection coefficient magnitude of the coupled structure for normal incidence in the working frequency range of 8-14 GHz is shown in Fig. 6. At the OFF state, namely, the situation of pixelated FSS combined with quartz tubes, a little absorption point of −6.6 dB appears around the central frequency of 12.2 GHz, which is the synthetic result of the modulation of EM wave by FSS and the structure reflection of the quartz tube. When the FSS and double-layer plasma arrays coexist, the reflection spectrum is far beneath that of the former. The wideband response occurs during the whole working frequency bands (below −6 dB), showing resonant frequencies of 9.6 GHz and 12.3 GHz with the corresponding absorption peak values of −38.5 dB and −12.4 dB, respectively. More concretely, the −10 dB frequency bandwidth for the primary resonance reaches 1.4 GHz, and the absorption band below −10 dB is marked in the figure.

To illustrate the joint attenuation effect of pixelated FSS and plasmas, additional comparisons of absorption are also given in Fig. 7. First, the effect of FSS and plasmas alone on the incident wave will cause two resonant peaks with 1.1 GHz apart. It is observed that the pixelated FSS does not show an excellent absorptive response below 10 GHz, while double-layer plasma arrays lead to an attenuation of more than −5 dB over the entire operating frequency. Second, the central frequency and the resonance effect of FSS change with and without quartz tubes. It can be attributed to the fact that the outside layer with quartz modifies the phase of EM waves. The exterior materials can modify the

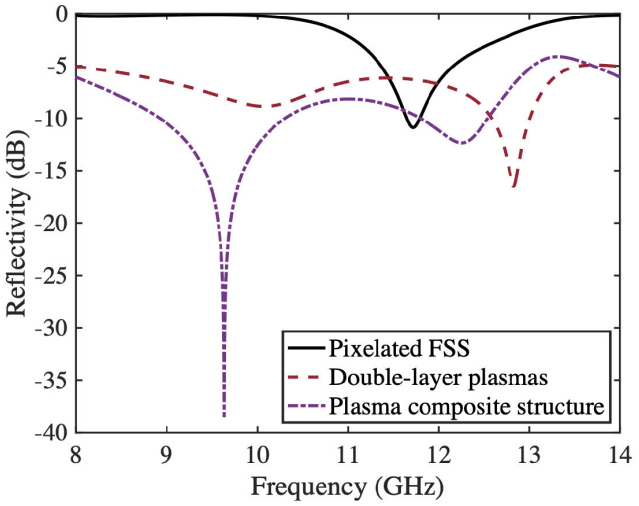

FIGURE 7. Comparisons of reflection response of the proposed coupled structure with pixelated FSS (PFSS) or plasma solely in experimental measurement.

phase of the incident wave so as to move the peak into the desired frequency range [28]. However, the cylindrical shape inevitably aggravates the scattering of EM waves. Third, one can see that the composite absorbing structure demonstrates remarkable resonance and bandwidth improvement. Apparently, double-layer plasmas on the grounded dielectric have an acceptable absorption value reaching −16.5 dB, and by adding the pixelated FSS, the attenuation is extended by almost 128 %. In addition, the resonance points of the coupled structure are not made in the region where they overlap each other. The frequency shift is due to the effect of combination and mutual coupling between different parts of the absorber. As the presence of multiple reflections, the incident wave interacts with each layer of the model, and it is enhanced by the total reflection of PEC. The combined attenuation effect of this structure is better than the effect of either plasma arrays or pixelated FSS solely.

B. RECONFIGURABILITY CHARACTERISTICS OF PLASMA COMPOSITE ABSORBING STRUCTURE COUPLED WITH PIXELATED FSS

Under the reduced power consumption of the proposed absorption structure, six working modes exhibiting reconfigurability characteristics are employed, as shown in Fig. 8. In general, the absorbing ability of the discharge on the interval side is better than that on the same side. Nevertheless, the coupled structure consisting of double-layer plasma arrays and pixelated FSS still exhibits unattainable performance at bandwidth and attenuation. According to the absorption theory of plasmas, the wave energy transfers to charged particles in the plasma, and subsequently to neutral particles (atoms and molecules) by elastic and inelastic collisions. It is thought that the hindering effect of plasmas on EM wave propagation decreases as the number of discharge tubes in working conditions decreases [30]. As the normal incident wave reaches the top layer, part of the wave is absorbed by plasmas, and the rest of the energy can be transmitted from the non-working discharge tubes since the dielectric constant of the gas inside the tube is extremely close to that of air when it is not working. In the case of the same-side discharge, nearly half of the incident energy is not exposed to plasmas and is only modulated by the FSS, which causes less effect on the attenuation of EM waves than the interval discharge. The comparison of the single-layer plasma with the ''ON'' state is as follows. When the plasma layer is closer to the wave source, there is a broadband absorption of -6dB exhibiting in most of the working frequency bands, accompanied by the absence of attenuation peaks. In the case of plasmas further away from the wave source, two resonance points with central frequencies of about 10.7 and 12.6 GHz exist, displaying the most significant attenuation value of −14.3 dB. It can be concluded that the proposed absorbing structure reconfigures in six modes as plasma layers switching with the same low power consumption: a broadband absorption at low frequencies, a broadband absorption at high frequencies, a broadband absorption without peaks, and an absorption with two peaks.

C. THE ABSORPTION ANALYSIS WITH CHANGING ARRANGEMENTS

In order to analyze the absorption mechanism of this ''sandwich-type'' structure, two other structures with the same profile are added for discussion seen in Fig. 9. In case 1, the pixelated FSS and plasma region modulate the incident wave successively, resulting in a resonance with a peak of −8.6 dB around 10.8 GHz. Conversely, when the incident wave first passes through thick plasma layers as shown in case 2, the reflection spectrum displays a wideband attenuation of about −5 dB over the whole frequency band, even with the presence of FSS. It can be seen that the front structures both react poorly in terms of broadband and attenuation, while the proposed structure maximizes the effectiveness of absorption over a wide frequency range in a relatively low profile.

To account for the absorption mechanism, the simulated average electric field distribution of each absorber at the cross-section in the y-z plane or on the FSS plane is shown in Figs. 10(a) to (f). The simulation is conducted with the frequency domain solver. The dielectric constant of plasma is defined by the Drude model, which the plasma frequency is assumed to be 6.8 GHz as well as the collision frequency is 7.4 GHz based on the calculation in Sec. II A. Compared with the electric field distribution of the sandwich-type structure at the y-z section, the decay of average superimposed electric fields of the other two structures are significantly weak in the free space, even though both are accompanied by the coupling effect, corresponding to the reflection feature in Fig. 9. In Fig. 10 (e), a strong electric field is generated at the contact region of the FSS and two separate plasma layers, indicating a large energy dissipation, which results in a decay of the superimposed field strength above the structure. Moreover, there are strong local field enhancements in the center of the pixelated cell in all three structures, while the

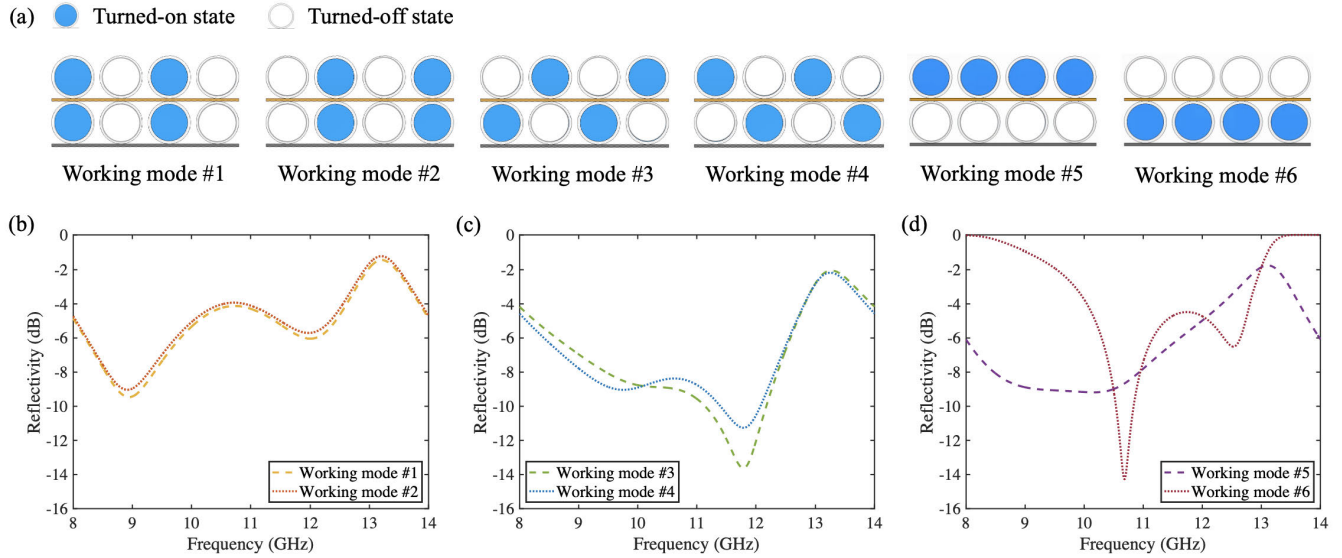

FIGURE 8. (a) Schematic of different working modes; (b)-(d) Reconfigurable reflection response of the proposed composite absorbing structure with six working modes in experimental measurement.

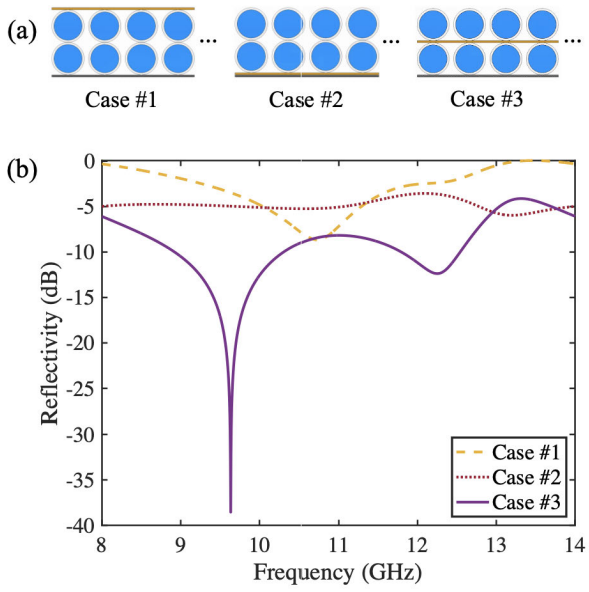

FIGURE 9. (a) Schematic of different array arrangements; (b) Comparisons of reflection response of the composite absorbing structure in three cases in experimental measurement.

average induced electric field of the proposed structure is maximum in the whole plane. The pixelated metal arrays in case 1 are induced with the electric field concentrated in the center due to the contact with the incident wave initially, with a large field gradient to the surrounding. However, the coverage region of the high-intensity field in case 2 is rarely resulting from absorption and scattering by thick plasma arrays. Due to the existence of the multilayer structure, part of the waves bounces back and forth in plasmas. An excessively thick plasma layer will cause the lower EM wave energy throughout to reach the FSS, reducing the modulation effect. On the other hand, the incident wave cannot achieve a deep penetration depth in plasma after being modulated by FSS. It can be seen that the strong coupling effect requires proper placement matching. The result can also explain the propagating features in Fig. 6 and Fig. 8(d), in which the absorption effect with double excited layer seems to be a superposition of monolayer excitation. The power loss density distribution of the proposed composite absorbing structure in the y-z plane is depicted in Fig. 10(g), indicating the sum of the electric and magnetic power dissipated inside the plasma. It is noticed that the projection of the y-z plane on the unit cell passes horizontally through the center of the surface. The inset not only demonstrates that the power dissipation is concentrated at the contact region between the plasma and FSS, but also emphasizes the absorption effect in the center of the FSS structure, which is exactly the result we expect. The local maximum achieves $1.54 \times 10^5\ W/m^{-3}$.

An interfacial void model for electromagnetic structures is proposed based on the field distribution. Unlike conventional interfaces of matter, the contact surface between electromagnetic layers is discontinuous and unitary, and for practical consideration, layers containing plasmas can only be used in a discrete manner. It leads to the existence of an interfacial void with little absorption contribution between the plasma layer and FSS layer, i.e., the air and the glass in this case, which modulates the incident wave through the curvature of plasma columns.

Figure 11 depicts the definition of the interfacial void by the incidence of EM waves and a simplified one-dimensional model, which the equivalent dielectric constant is denoted by ε_{eff}. As dissipative media, plasmas and the FSS layer sandwich the interfacial void zone, which is dominated by the dielectric loss. Periodic changes in topology lead to regular variations in ε_{eff}, and most dielectric materials have few losses so that the attenuation caused by the interfacial void under the plane wave condition is related to the wave number

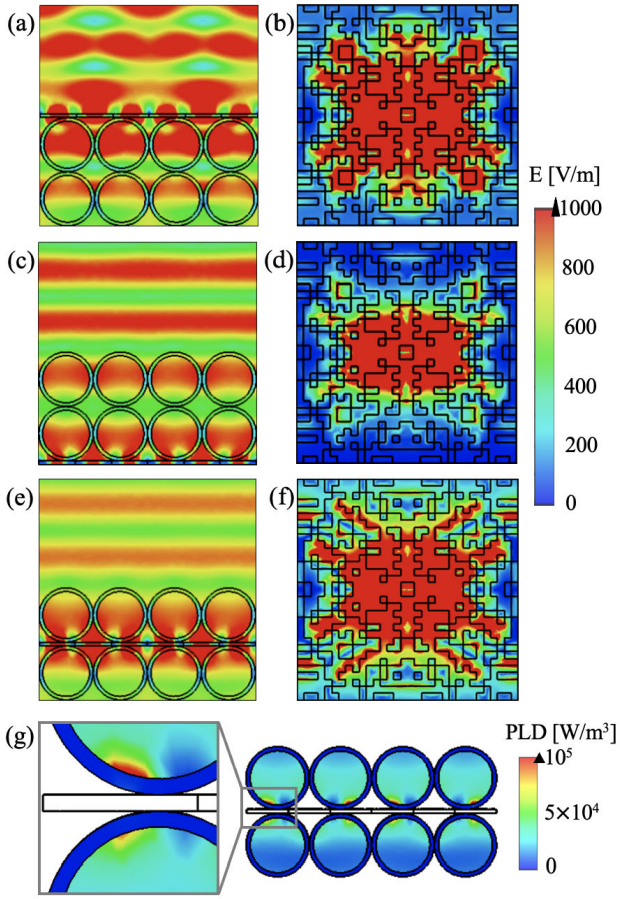

FIGURE 10. Simulated electric field distribution (excluding time phase) of three absorbers and the power loss density of the proposed structure observed at respective resonance points. (a), (c), and (e) E-field distribution of three structures in the y-z plane, respectively; (b), (d), and (f) E-field distribution of three structures on the FSS plane, respectively; (g) power loss density of the proposed composite absorbing structure in the y-z plane and the partially enlarged illustration.

and the equivalent loss tangent [31]

$$\alpha \sim k(tan\delta)_{eff}, \tag{5}$$

Combining three matching layouts under the same profile, the following analysis can be derived. Firstly, the larger the contact area there is, the more wave energy is dissipated. The sandwich-type structure exists with two times the interfacial void area than the other two cases. In addition, periodic changes in the interfacial void affect the interfacial effects of the composite structure. The morphology of the plasma layer controls the scale of the interfacial void and thus influences interfacial capacitance. Given that the interfacial void cannot be obliterated, combining the particularity of the interfacial void to rationalize the absorber's topology can effectively control the absorption effect.

D. POWER CONSUMPTION ESTIMATION

It is known that plasmas are reconfigurable due to the physical parameters and input power, and some special applications, such as flying vehicle surfaces, require high attenuation with

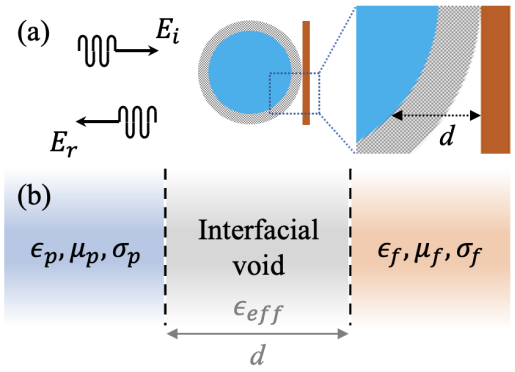

FIGURE 11. Schematic diagram of (a) the two-dimension interfacial void and (b) the simplified one-dimension interfacial void.

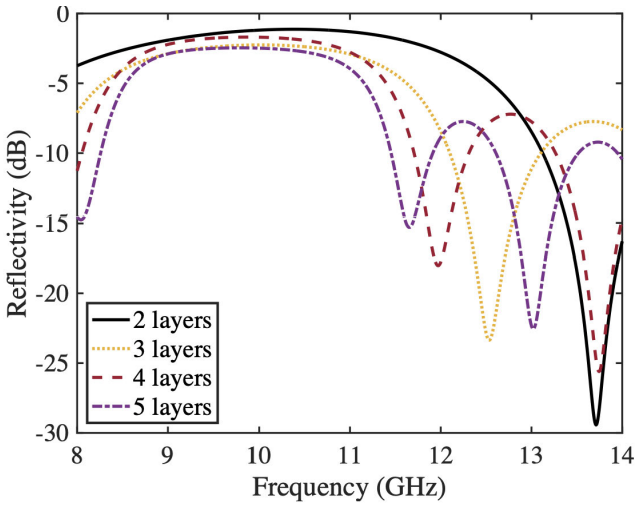

FIGURE 12. Simulated reflection (S11) for plasma periodic structures with different layers.

power and profile limitations. Thus, it is necessary to evaluate power conservation in this design.

Power required to maintain the electron density over the volume V is given by [4]

$$P = \frac{n_e E_i V}{\tau} = k_r {n_e}^2 E_i V, \tag{6}$$

where E_i is the ionization potential, τ is the plasma life time, and k_r is the recombination rate.

It is observed that the power is positively correlated with the volume assuming the uniform distribution and the same physical parameters of each enclosed plasma. The reflection characteristics for plasma periodic structures with different numbers of layers are given in Fig. 12, in which the pixelated FSS is absent. As the number of layers increases, the absorption center frequencies move towards the lower-frequency end and the absorption peak gradually decreases, with multiple peaks appearing from the fourth layer. The average reflection tends to decrease and then increase, achieving the same level as the proposed coupled structure at the fifth layer in the simulation. In other words, ignoring the thickness of the pixelated FSS, it gives a rough estimation that the periodic plasma arrays without coupling require 2.5 times the power

than the hybrid design, including the height

$$\frac{P_{plasma}}{P_{hybrid}} = \frac{H_{plasma}}{H_{hybrid}} = \frac{5}{2}, \tag{7}$$

with P_{plasma} and H_{plasma} being the Power consumption and the height of the simulated plasma periodic structures, P_{hybrid} and H_{hybrid} being the Power consumption and the height of the proposed composite absorbing structure with double-layer plasma arrays sandwiched the pixelated FSS.

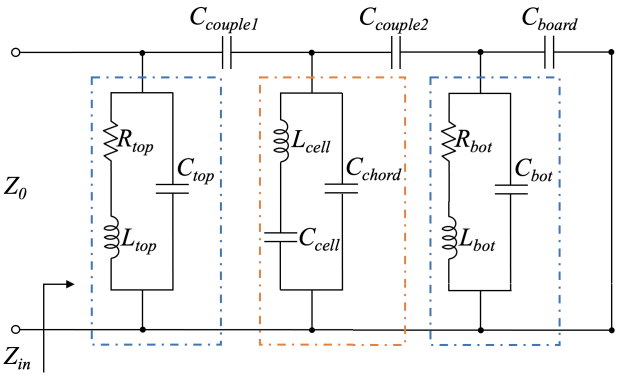

FIGURE 13. The equivalent circuit model of the proposed multilayer absorbing structure based on transmission line approach.The blue dashed boxes represent plasma layers, while the orange one represents the FSS layer.

E. EQUIVALENT CIRCUIT MODELING

To provide an excellent physical insight into the design properties of the structure, a lumped circuit model is adopted based on the transmission line theory in Fig. 13. It is assumed that the FSS layer embedded between two plasma layers has a similar configuration in both layers, which the coupling effect is experienced by the mutual capacitance with the resonant eddy currents in plasmas nearby ($C_{couple1}$ and $C_{couple2}$). For each layer of the plasma tube array, there is an intrinsic impedance in the axial direction of the tube due to the plasma conductivity, i.e., a series of resistive $R_{top(bot)}$ and inductive $L_{top(bot)}$, and the mutual inductance in the radial direction is represented by a parallel capacitive $C_{top(bot)}$. An equivalent circuit model of the periodic metallic structure in a unit cell consists of a series of inductive L_{cell} and capacitive C_{cell}, ignoring the effect of surface resistivity and the loss of medium. Each unit also has capacitive interactions C_{chord} with other unit structures. There is another capacitive interaction C_{board} that needs to be considered, which is the interaction between the absorber and the total reflective metal plate [6]. In addition, Z_0 is the wave impedance in the free space and is equal to 377 Ω.

The lumped parameters of the equivalent circuit model are determined so that an acceptable agreement is observed between the results of the equivalent circuit model and those of the experimental results, as shown in Table I. The equivalent resistance of glow discharge plasma can be approximated by the resistivity model [32]

$$\rho \approx \frac{\pi e^2 m^{1/2}}{(4\pi\varepsilon_0)^2 (KT_e)^{3/2}} ln\Lambda, \tag{8}$$

where

$$\Lambda = \lambda_D / r_0 = 12\pi n_e \lambda_D^3, \tag{9}$$

with Λ representing the maximum impact parameter, which depends on the electron number density and Debye length. In this experiment, $ln\Lambda$ is given to be 10, and the electron temperature T_e is determined to be 0.34-1 eV through the conventional microwave diagnostic method. Thus, the resistance of each plasma tube ranges between 0.3 Ω and 3.1 Ω.

Three deductions can be summarized by comparing the circuit parameters of the top and bottom plasma layers. First, plasma at the top layer has a more negligible impedance affected by the coupling effect with the periodic metallic structure. It is known that the electron number density in the tube increases directly, leading to an increase in conductivity and a decrease in impedance. Through the parameter sensitivity analysis, microwave absorption is enhanced by the reduction of the resistance value of plasmas. Second, the inductive impedance of the top layer is greater as the electric field increases. Through parameter sensitivity analysis, it can be seen that as the inductance decreases, the absorption center frequency will shift to the high-frequency end, and otherwise, it shifts to the low-frequency end. Finally, the top layer has a stronger interaction between tubes, which is exhibited by the reduction of the capacitance. The parameter sensitivity analysis shows that as the capacitance decreases, the absorption center frequency will also shift to the high-frequency end; otherwise, it shifts to the low-frequency end. Corresponding to the electric field analysis in Fig. 10, the inductive impedance of the top layer is greater, and the capacitive impedance is smaller, which results in stronger resonant eddy currents. The control of frequency shift and bandwidth results from multi-parameter synthesis [6].

Furthermore, in conjunction with the interfacial void model presented in the previous section, the two coupling capacitances show the interfacial effect of interfacial voids. The coupling capacitance of the upper layer is smaller, showing the tighter interaction between the plasma and the FSS. If the curvature radius of the plasma tube increases, and thus the scale of the interfacial void increases, leading to a decrease in the interfacial capacitance. Figure 14 documents changing processes of S-parameters for several sets of typical values, in which the solid line plots the initial case. In general, as C_{couple} decreases, the absorption center frequency will shift to the high-frequency end, and otherwise, it shifts to the low-frequency end. Thereinto, $C_{couple1}$ shows a more sensitive response to the EM wave; however, $C_{couple2}$ has little effect on microwave absorption until below 0.1. The upper plasma layer makes the effect of the interfacial void more significant due to being closer to the wave source, but the lower plasma layer is not negligible either. It demonstrates that the shape of the designed layer also influences absorption characteristics.

At normal incidence, the grating lobes wavelength equals the FSS periodicity, leading to a 30 GHz propagating Floquet harmonic in the proposed pixelated FSS [33]. However, when the FSS is embedded with dielectric media, the

TABLE 1. The main equivalent elements and the corresponding numerical values used in the model.

Parameters	Values
R_{top} (Ω)	0.46
L_{top} (nH)	6.71
C_{top} (fF)	5.11
R_{bot} (Ω)	0.79
L_{bot} (nH)	0.20
C_{bot} (fF)	153.20
$C_{couple1}$ (fF)	33.06
$C_{couple2}$ (pF)	2.65
C_{board} (pF)	0.78
L_{cell} (nH)	10.53
C_{cell} (fF)	901.08
C_{chord} (fF)	0.39

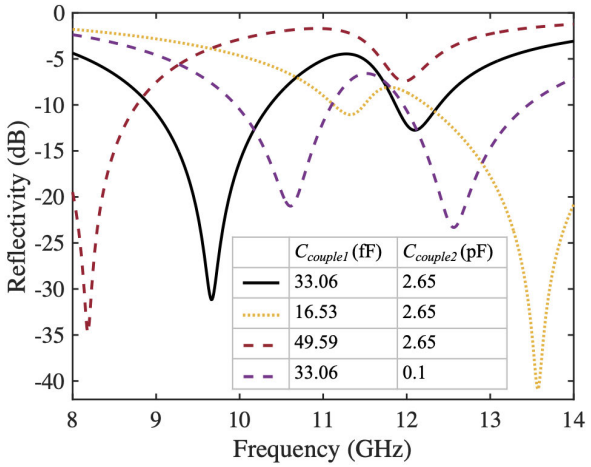

FIGURE 14. S-parameters for the circuit parameter adjustment of coupling capacitances.

first high-order phenomenon is represented by the onset of trapped dielectric modes (or trapped surface waves) that occur well below the propagation of the first grating lobe. Since the "quasi-plasma" high-density metallic periodic structure has a random distribution with tiny discrete elements, the frequency-dependent impedance network with a multi-scale characteristic structure is discussed below.

In order to describe the response behavior of the pixelated FSS with continuously adjustable parameters, several additional elements are necessary for the circuit model, which is characterized as frequency-dependent additional terms. In addition to the intrinsic lumped elements (L_{cell}, C_{cell} and C_{chord}), the capacitive impedance of the FSS coupled to plasma layers on both sides ($C_{couple1}$ and $C_{couple2}$) should also have frequency-dependent characteristics. Taking L_{cell} as an example, the improved circuit model is expressed as

$$L_{cell}(\omega) = L_{cell0} + P(\omega)\hat{L_{cell}}, \tag{10}$$

where

$$P(\omega)\hat{L_{cell}} < L_{cell0}, \tag{11}$$

with L_{cell0} referring to the value in Table 1. The frequency-dependent excitation factor $P(\omega)$ is assumed to be the product of the weight p and the frequency for simplicity. The perturbation term $\hat{L_{cell}}$ is assumed to be one-tenth of the

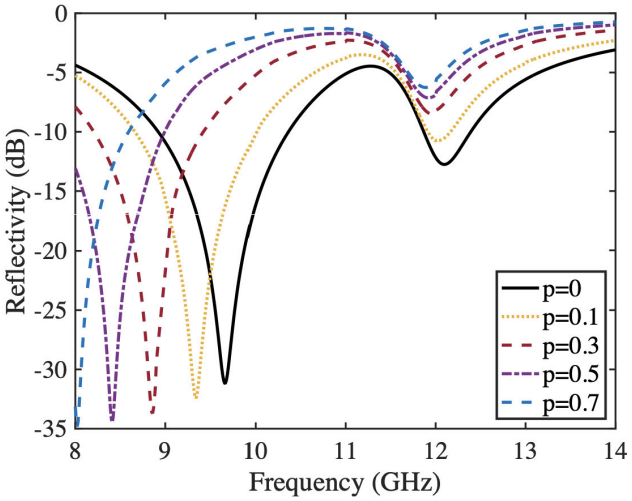

FIGURE 15. S-parameters for frequency-dependent circuit parameter adjustment.

base value, which is acceptable for discussion with a definite level.

Four statuses have been calculated based on the improved lumped circuit model with different weights, and the results are shown in Fig. 15. The status without frequency independence is plotted by the solid line. It is observed that as the weight increases, the first absorption center frequency shifts toward the low-frequency end and the absorption enhances, while the second absorption center frequency has a slightly reduced shift and the absorption decreases. As the frequency dependence increases, the frequency response characteristics of the operating band gradually disappear. The approach is a matching procedure mainly aiming at understanding physical mechanisms in the dynamic frequency response of the coupled structure.

IV. CONCLUSION

In this study, a novel design of a reconfigurable composite absorbing structure is implemented to control the propagation of EM waves in 8-14 GHz bands. The FD-CGAN model based on conditional GANs is proposed to generate optimal geometric structures according to the adaptability of the coupled structure. The incident wave power is reduced significantly in a wide frequency bandwidth via a proper design of the absorber with enclosed plasmas and pixelated FSS, accompanied by the dynamically adjustable attenuation level. Measurements indicate that the addition of metallic periodic structures makes the coupling absorption effect surpass that of either pixelated FSS or plasma solely, and the reconfigurability is validated in six working modes. The reflection responses of the three absorbers with various arrangements demonstrate that the "sandwich-type" structure maximizes the effectiveness of absorption over a wide frequency range in a relatively low profile, accompanied by the electric field and the power loss density distribution. An interfacial void model is proposed to assist in the design of the composite absorbing structure. The power consumption estimation shows that the

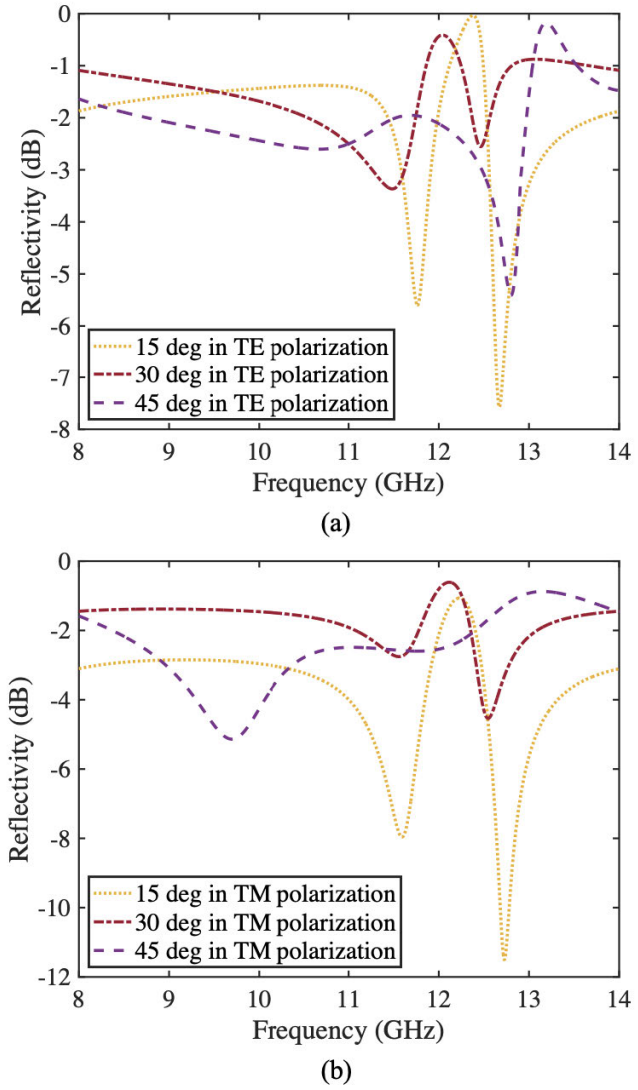

FIGURE 16. Measured reflectivity of the design of the case 3 in Fig.9 for various oblique angles of incident wave in (a) TE polarization and (b) TM polarization.

periodic plasma arrays without coupling require 2.5 times the power to achieve the same absorption as the hybrid design. The coupled structure is described based on the transmission line method, which characteristic lumped elements have been analyzed using experimental data fitting, and the frequency-dependent impedance network with a multi-scale characteristic structure is discussed. As the plasma generation technology becomes mature, the method in this paper is promising to be introduced into the application such as plasma-based stealth technology. In addition, combining DL with the coupled absorber structure design is of practical significance to overcome the limitation of the traditional rule-based strategies with trial-and-error.

APPENDIX
OBLIQUE INCIDENT PERFORMANCE

In addition to the propagation of normally incident EM waves in the proposed reconfigurable absorber, we have also investigated the oblique incident performance at various angles in both transverse electric (TE) and transverse magnetic (TM) polarizations. The measured results are depicted in Fig. 16, which shows the stable dual resonance peaks up to 30° with center frequencies slightly shifted. While at an incident angle of 45°, especially for the TM polarization, the absorption response produces large frequency shifts, which may be due to the cavity resonance effect of the array structure at large angles.

REFERENCES

[1] R. J. Vidmar, "On the use of atmospheric pressure plasmas as electromagnetic reflectors and absorbers," *IEEE Trans. Plasma Sci.*, vol. 18, no. 4, pp. 733–741, Aug. 1990.
[2] T. Jiang and Z. Hou, "A reconfigurable frequency selective structure using plasma arrays," *AIP Adv.*, vol. 10, no. 6, Jun. 2020, Art. no. 065102.
[3] R. Kumar and D. Bora, "A reconfigurable plasma antenna," *J. Appl. Phys.*, vol. 107, no. 5, p. 3272, 2010.
[4] H. Singh, S. Antony, and R. M. Jha, *Plasma-Based Radar Cross Section Reduction*. Singapore: Springer, 2016, pp. 1–46.
[5] K. R. Stalder, R. J. Vidmar, and D. J. Eckstrom, "Observations of strong microwave absorption in collisional plasmas with gradual density gradients," *J. Appl. Phys.*, vol. 72, no. 11, pp. 5089–5094, 1992.
[6] Y. Hu, M. Fang, Y. Qian, M. Liu, H. Shen, and Z. Hou, "Electrode cooling and microwave absorption by phase change fluid discharge plasma," *IEEE Trans. Microw. Theory Techn.*, vol. 70, no. 7, pp. 3472–3485, Jul. 2022.
[7] L. W. Cross, M. J. Almalkawi, and V. K. Devabhaktuni, "Development of large-area switchable plasma device for X-band applications," *IEEE Trans. Plasma Sci.*, vol. 41, no. 4, pp. 948–954, Sep. 2013.
[8] M. Z. Joozdani and M. K. Amirhosseini, "Wideband absorber with combination of plasma and resistive frequency selective surface," *IEEE Trans. Plasma Sci.*, vol. 44, no. 12, pp. 3254–3261, Dec. 2016.
[9] K. Payne, E. F. Peters, J. Brunett, D. K. Wedding, C. A. Wedding, and J. H. Choi, "Second-order plasma enabled tunable low-profile frequency selective surface based on coupling inter-layer," in *Proc. 46th Eur. Microw. Conf. (EuMC)*, Oct. 2016, pp. 309–312.
[10] K. Payne, J. K. Lee, K. Xu, and J. H. Choi, "Low-profile plasma-based tunable absorber," in *Proc. IEEE Int. Symp. Antennas Propag. USNC/URSI Nat. Radio Sci. Meeting*, Jul. 2018, pp. 2065–2066.
[11] K. Payne, K. Xu, J. H. Choi, and J. K. Lee, "Plasma-enabled adaptive absorber for high-power microwave applications," *IEEE Trans. Plasma Sci.*, vol. 46, no. 4, pp. 934–942, Apr. 2018.
[12] B. A. Munk, *Freq. Selective Surfaces: Theory Design*. Hoboken, NJ, USA: Wiley, 2005.
[13] D. G. Holtby, K. L. Ford, and B. Chambers, "Genetic algorithm optimisation of dual polarised pyramidal absorbers loaded with a binary FSS," in *Proc. Loughborough Antennas Propag. Conf.*, Nov. 2009, pp. 3878–3880.
[14] P. Naseri and S. V. Hum, "A generative machine learning-based approach for inverse design of multilayer metasurfaces," *IEEE Trans. Antennas Propag.*, vol. 69, no. 9, pp. 5725–5739, Sep. 2021.
[15] I. Goodfellow, J. Pouget-Abadie, M. Mirza, B. Xu, D. Warde-Farley, S. Ozair, A. Courville, and Y. Bengio, "Generative adversarial nets," in *Proc. 27th Int. Conf. Neural Inf. Process. Syst.*, 2014, pp. 2672–2680.
[16] Z. Liu, D. Zhu, S. Rodrigues, K. Lee, and W. Cai, "Generative model for the inverse design of metasurfaces," *Nano Lett.*, vol. 10, no. 18, p. 65706576, May 2018.
[17] Z. Zhang, D. Han, L. Zhang, X. Wang, and X. Chen, "Adaptively reverse design of terahertz metamaterial for electromagnetically induced transparency with generative adversarial network," *J. Appl. Phys.*, vol. 130, no. 3, Jul. 2021, Art. no. 033101.
[18] J. A. Hodge, K. V. Mishra, and A. I. Zaghloul, "RF metasurface array design using deep convolutional generative adversarial networks," in *Proc. IEEE Int. Symp. Phased Array Syst. Technol. (PAST)*, Oct. 2019, pp. 1–6.
[19] Y. Mao, Q. He, and X. Zhao, "Designing complex architectured materials with generative adversarial networks," *Sci. Adv.*, vol. 6, no. 17, Apr. 2020, Art. no. eaaz4169.
[20] D. J. Kern and D. H. Werner, "A genetic algorithm approach to the design of ultra-thin electromagnetic bandgap absorbers," *Microw. Opt. Technol. Lett.*, vol. 38, no. 1, pp. 61–64, Jul. 2003.

[21] S. Genovesi, R. Mittra, A. Monorchio, and G. Manara, "Particle swarm optimization for the design of frequency selective surfaces," *IEEE Antennas Wireless Propag. Lett.*, vol. 5, pp. 277–279, 2006.
[22] B. Wang, J. A. Rodríguez, O. Miller, and M. A. Cappelli, "Reconfigurable plasma-dielectric hybrid photonic crystal as a platform for electromagnetic wave manipulation and computing," *Phys. Plasmas*, vol. 28, no. 4, Apr. 2021, Art. no. 043502.
[23] G. J. M. Hagelaar and L. C. Pitchford, "Solving the Boltzmann equation to obtain electron transport coefficients and rate coefficients for fluid models," *Plasma Sources Sci. Technol.*, vol. 14, no. 4, pp. 722–733, Oct. 2005.
[24] M. K. Howlader, Y. Yang, and J. R. Roth, "Time-resolved measurements of electron number density and collision frequency for a fluorescent lamp plasma using microwave diagnostics," *IEEE Trans. Plasma Sci.*, vol. 33, no. 3, pp. 1093–1099, Jun. 2005.
[25] A. Ghayekhloo, A. Abdolali, and S. H. Mohseni Armaki, "Observation of radar cross-section reduction using low-pressure plasma-arrayed coating structure," *IEEE Trans. Antennas Propag.*, vol. 65, no. 6, pp. 3058–3064, Jun. 2017.
[26] B. Chaudhury and S. Chaturvedi, "Three-dimensional computation of reduction in Radar cross section using plasma shielding," *IEEE Trans. Plasma Sci.*, vol. 33, no. 6, pp. 2027–2034, Dec. 2005.
[27] X. Ren, C. Liu, and M. Zeng, "S11 parameter calculation of frequency selective surface based on deep learning," *J. Phys., Conf. Ser.*, vol. 1865, no. 4, Apr. 2021, Art. no. 042022.
[28] C.-X. Yuan, Z.-X. Zhou, J. W. Zhang, X.-L. Xiang, Y. Feng, and H.-G. Sun, "Properties of propagation of electromagnetic wave in a multilayer radar-absorbing structure with plasma- and radar-absorbing material," *IEEE Trans. Plasma Sci.*, vol. 39, no. 9, pp. 1768–1775, Sep. 2011.
[29] F. Costa, A. Monorchio, and G. Manara, "Efficient analysis of frequency-selective surfaces by a simple equivalent-circuit model," *IEEE Antennas Propag. Mag.*, vol. 54, no. 4, pp. 35–48, Sep. 2012.
[30] Y. Liang, Z. Liu, L. Lin, J. Peng, R. Liu, and Q. Lin, "Transmission characteristics of electromagnetic waves in 2D tunable plasma photonic crystals," *Appl. Opt.*, vol. 60, no. 9, p. 2510, 2021.
[31] D. M. Pozar, *Microwave Engineering*. Hoboken, NJ, USA: Wiley, 2006.
[32] F. F. Chen, *Introduction to Plasma Physics and Controlled Fusion*, vol. 1, 2nd ed. New York, NY, USA: Plenum Press, 1984, ch. 5, pp. 178–183.
[33] F. Costa, A. Monorchio, and G. Manara, "An overview of equivalent circuit modeling techniques of frequency selective surfaces and metasurfaces," *Appl. Comput. Electromagn. Soc. J.*, vol. 29, no. 12, pp. 960–976, Dec. 2014.

MENGJIE YU received the B.S. degree in electronic science and technology from the School of Microelectronics, Tianjin University, China, in 2016. She is currently pursuing the Ph.D. degree in electronic science and technology with Shanghai Jiao Tong University, Shanghai, China. Her research interests include the interaction of non-equilibrium atmospheric plasma with water and the absorption characteristics of the plasma composite structure.

HAITAO WANG received the Ph.D. degree in electronic science and technology from Shanghai Jiao Tong University, Shanghai, China, in 2021. His research interests include non-equilibrium atmospheric plasma in air, absorption characteristics of the plasma composite structure, and plasma flow control.

XIANGXIANG GAO received the B.S. degree in metal materials and engineering from the School of Mechanical and Electrical Engineering, Hohai University, China, in 2018. She is currently pursuing the Ph.D. degree in electronic science and technology with Shanghai Jiao Tong University, China. Her research interest includes the engineering applications of artificial intelligence.

XI REN received the M.S. degree in electronic science and technology from the School of Electronic Information and Electrical Engineering, Shanghai Jiao Tong University, Shanghai, China, in 2020. His research interest includes the design of the frequency selective surface based on deep learning.

ZUNYI TIAN received the Ph.D. degree in electronic science and technology from Shanghai Jiao Tong University, Shanghai, China, in 2022. His research interests include electron transmission window, electron beam plasma, and MEMS device.

HENGGAO DING, photograph and biography not available at the time of publication.

ZHONGYU HOU received the Ph.D. degree in electronic science and engineering from Shanghai Jiao Tong University. He is currently a Professor at Shanghai Jiao Tong University. He is also working on the development of a new research methodology incorporating artificial intelligent techniques. His research interests include plasma science and technology in the application context of microwave technology, aerodynamics, environment, and MEMS-based sensors and actuators.